scientific reports

Check for updates

OPEN

Multi-wavelength imaging photoplethysmography for non-invasive and non-contact assessment of burn severity

You-rim Park & Joo Beom Eom

We report a non-contact burn severity assessment system using the image-based photoplethysmography (IPPG) technique by fabricating a multi-wavelength imaging system. In this burn assessment system, four wavelengths (visible light wavelengths of 405 nm, 520 nm, 660 nm, and near-infrared wavelength of 940 nm) were used, and burn severity was identified based on the fact that each wavelength has different penetration depths. Each wavelength was set to irradiate with the same optical power (1 mW/cm²), and IPPG was acquired using images captured at 35 frames per second for wavelengths with different penetration depths. To measure burn severity, we created burn lesion models using hairless mice. For each degree of burn, we acquired images of the burn area at four different wavelengths, measured IPPG from the acquired images, and observed the signal change at each wavelength to evaluate burn severity. In addition, while monitoring the healing process, we observed that IPPG recovered as the blood flow in the tissue normalized. Through the results of this study, we expect that IPPG technology will be used not only as a non-contact technology to evaluate burn severity, but also as a new method to monitor the burn recovery process in real time.

Keywords Imaging photoplethysmography, Burn depth, Dual-camera, Multi-wavelength, Laser diodes

Burns can be caused by heat, freezing, electricity, chemicals, radiation, or friction, and depending on their location and depth, burn patients may experience life-threatening complications[1]. Thermal burns account for the majority of reported skin burns. Local wounds from thermal burns are caused by thermal necrosis of cells and are classified as superficial, partial-thickness, or full-thickness burns depending on the depth of the injury[2,3].

First-degree (superficial) burns affect only the outermost layer of the skin, the epidermis (0.05–0.15 mm). Symptoms of this type of burn include redness and swelling of the skin due to erythema. Second-degree (partial-thickness) burns affect both the epidermis and the dermis and can be classified into superficial partial-thickness burns, which damage only the superficial layer of the dermis, and deep partial-thickness burns, which extend damage to the deeper layers of the dermis (1–4 mm). These burns cause symptoms such as separation of the epidermis and dermis, collagen degeneration in the dermal layer, and the appearance of pain, redness, and blisters. After healing, the skin may become discolored, and scarring can occur. Third-degree burns and higher, also known as full-thickness burns, extend beyond the epidermis and dermis to involve subcutaneous tissues, including underlying fat, muscles, tendons, and even bones (greater than 4 mm). These wounds heal through contraction along with epithelialization from the wound margins, leaving scars, and complete natural healing is not possible without surgical intervention[3–6].

Classifying burns is crucial for diagnosing the injury, selecting appropriate treatment methods, and anticipating and managing infections and risks that may arise during the healing process. However, there is currently no standardized criteria for diagnosing burns due to the wide variety of wound causes and the complexity that results in numerous types of injuries[7]. Burns are typically classified by surgeons based on parameters such as surface area, depth, and wound location. Using burn depth as one of these parameters to classify burn severity is an important clinical goal in managing burn patients[7–9].

Widely used methods for assessing the depth of burn injuries are clinical evaluation and histological analysis[8]. Current clinical evaluations rely on subjective assessments of the wound's external characteristics[10]. Clinical judgment can diagnose very deep or very shallow burns, but the accuracy of intermediate-depth burns (second-degree burns) is only 60–80%, with the accuracy being even lower when the diagnosis is made within

Department of Biomedical Science, College of Medicine, Dankook University, 119 Dandae-ro, Dongnam-gu, Cheonan 31116, Korea. email: jbeom@dankook.ac.kr

the first 48 h after the burn[11]. However, since second-degree burns account for a significant portion of burn cases, accurately diagnosing them is crucial as it directly impacts treatment and prognosis. Because the accuracy of clinical judgment is low, histological analysis, which can distinguish necrotic tissue from healthy tissue, is performed and is considered the gold standard for diagnosing second-degree burns. However, this histological analysis method has the disadvantage of being invasive and taking a considerable amount of time to confirm the results[12]. Therefore, a technique to accurately and noninvasively assess the depth of burn wounds is needed.

Accordingly, many studies have been conducted on non-invasive methods for measuring burn depth, with tissue perfusion measurement being a representative approach. Since burns damage the blood vessels of the skin, this is considered one of the most reliable indicators for determining the extent of burn damage. Therefore, measuring tissue perfusion can be used as a potential tool for assessing burn depths[8,13]. Various techniques have been developed as methods for measuring tissue perfusion, such as infrared (IR) thermography[14], angiography[15], laser doppler imaging (LDI)[16,17], laser speckle contrast imaging (LSCI)[18] and hyperspectral imaging (HSI)[19]. A Research group using IR thermography has quantitatively assessed burn depth using temperature as a parameter. A significant difference in average temperature was observed between second-degree and third-degree burns, allowing for their distinction[14]. However, this method indirectly evaluates blood flow using temperature alone and is vulnerable to changes in ambient temperature, which may result in low accuracy. Another research group used a fluorescence technique using indocyanine green (ICG) to evaluate skin perfusion[15]. ICG fluorescence images showed a clear difference between superficial partial thickness burns and full thickness burns. However, this method is inconvenient because it requires considering the time delay between dye injection and fluorescence emission, rather than the assuming immediate fluorescence emission. In studies using LDI, blood flow was measured to assess tissue perfusion and evaluate burn severity. Blood flow decreased in the order of superficial partial thickness, deep partial thickness, and full thickness burns[16]. However, although this method has the advantage of being a non-invasive perfusion imaging method, it requires contact between the probe and the skin, which can affect the burn wound. On the other hand, non-contact LDI has been developed to overcome this limitation, allowing for the measurement of tissue perfusion without direct contact. However, due to the use of a single wavelength, this method is primarily limited to measuring blood flow dynamics based on doppler shifts and does not provide depth-specific perfusion information[17]. A study using LSCI measured tissue perfusion across the entire area through imaging, allowing for the prediction of burn wound healing potential[18]. However, like LDI, LSCI uses a single wavelength, which limits its ability to provide depth-specific perfusion information. On the other hand, the group that used HSI demonstrated that it can evaluate three different burn depths by measuring parameters such as hemoglobin levels and tissue oxygen saturation[19]. While HSI is effective for acquiring detailed tissue information, it requires huge equipment and involves slow data processing, making it less practical for rapid assessment or bedside use in clinical settings.

To complement the limitations of existing studies, we propose a novel concept for a burn severity measurement system that can measure burn depth in a non-invasive and non-contact manner. The method is to use the image-based photoplethysmography (IPPG) method and monitor burn severity and recovery through it. IPPG is a technology that detects dynamic changes in intravascular blood volume by measuring changes in light absorption using a camera and a light source[20–23]. Unlike existing studies, IPPG technology offers the advantage of non-contact, real-time assessment of blood volume changes in the skin. Furthermore, the use of multiple wavelengths enables the assessment of burn severity by analyzing the extent of blood flow damaging at varying tissue depths. In this technology, we used the different penetration depths of light inside the skin, which are caused by different scattering and absorption coefficients of visible light and near-infrared light[24–26].

Since light penetration depth varies depending on wavelength due to differences in absorption and scattering properties, we leveraged this principle to assess burn severity. Shorter wavelengths, such as blue and green light, are strongly absorbed by melanin and hemoglobin and primarily reflect changes in superficial layers, whereas longer wavelengths, such as red and near-infrared, penetrate deeper into the tissue. This is due to the relatively low attenuation coefficients of biological tissue components, such as melanin, water, and collagen, in these wavelengths, which results in minimal absorption and scattering. By utilizing these wavelength-dependent penetration characteristics, we aimed to distinguish burns at different depths more accurately[27]. Although the penetration depth may vary depending on the measurement methods used in previous studies, in the spectral range used in our experiment, the maximum penetration depth into skin tissue was approximately 0.3–1 mm at the blue wavelength (i.e., 405 nm), 0.3–2.5 mm at the green wavelength (i.e., 520 nm), 1.8–4.5 mm at the red wavelength (i.e., 660 nm), and 2.5–5 mm at the near-infrared wavelength (i.e., 940 nm)[25–33]. To evaluate the feasibility of this proposed method in an animal model before applying it to humans, we conducted experiments on mice. Considering the thin skin of mice, we applied the lowest light power (1 mW/cm^2) capable of measuring IPPG signals at each wavelength. Consequently, the maximum penetration depth for each wavelength in our experiment was determined at this fixed power. In IPPG signal-based research, the measurement depth of light returning through blood vessels is more critical than the maximum penetration depth itself, as IPPG relies on detecting signals from light that has traveled through blood vessels.

To verify the performance of the proposed system, we created burn lesion models corresponding to each burn degree using hairless mice and analyzed IPPG signals at various wavelengths. We also repeated the measurements during the recovery process. Through these experimental results, we confirmed that the proposed technology has potential as a device for measuring burn severity in a non-invasive, non-contact way.

Methods

Imaging system with multiple wavelength light sources for burn depth assessment

The system for evaluating the burn depth was fabricated as shown in Fig. 1 and consists of laser light sources and a camera system. The light sources employed were laser diodes emitting at specific wavelengths: 405 nm (blue; WSLP-405–400 m-50 M; Wavespectrum, Beijing, China), 520 nm (green; LDX-3102-520-FCP; LDX

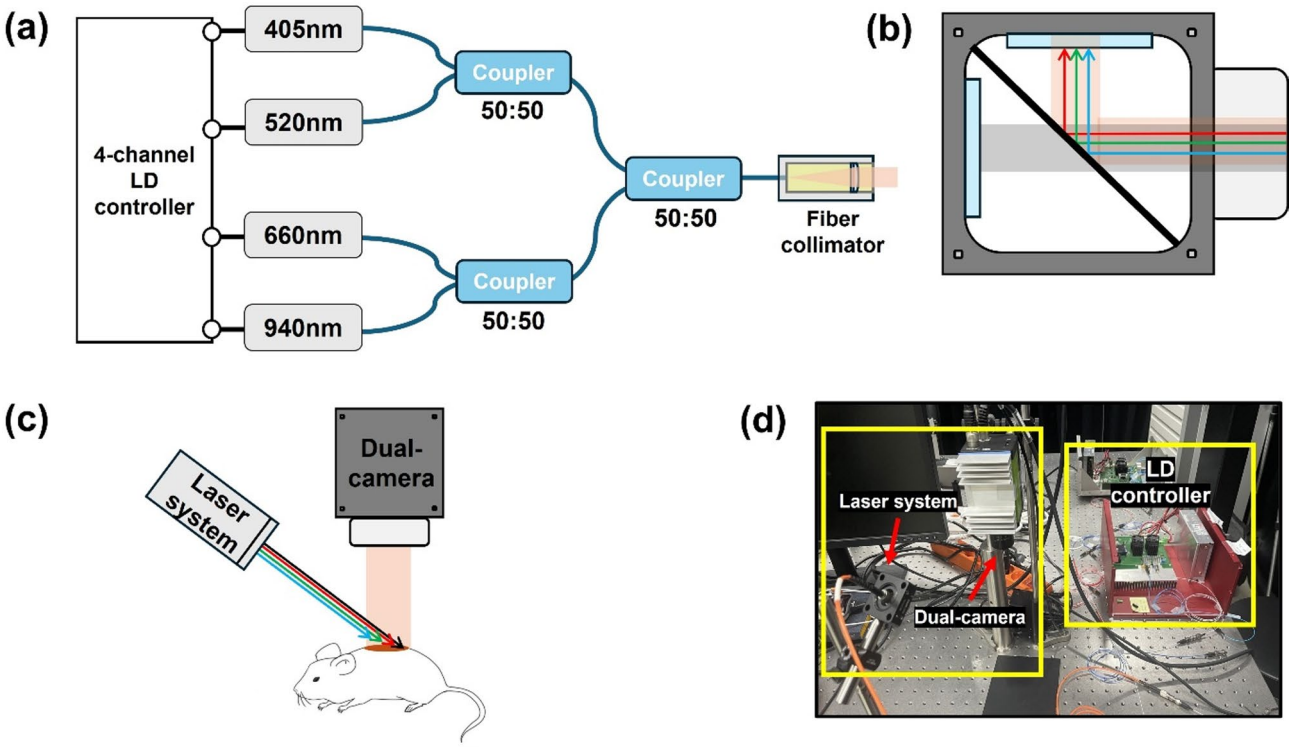

Fig. 1. Light source and camera system for burn depth assessment (**a**) The schematic diagram of the laser system combining multiple wavelengths (**b**) The schematic diagram of a dual-camera accommodating visible and near-infrared light (**c**) The schematic diagram of the imaging system **(d)** Experimental system setup.

Optronics Inc., Tennessee, U.S.), 660 nm (red; LDX-3115-660-FCP; LDX Optronics Inc., Tennessee, U.S.), and 940 nm (near-infrared; LDX-3515-940-FCP; LDX Optronics Inc., Tennessee, U.S.). As shown in Fig. 1a, the four fiber-coupled laser diodes were combined into a single optical path using 2 × 2 multimode fiber couplers (TM200R5S2B; Thorlabs, New Jersey, U.S.). A fiber collimator (CFC8-B; Thorlabs, New Jersey, U.S.) was mounted at the fiber output to transform the emitted light into a collimated beam. The collimated beam was made selectively switchable between wavelengths using a 4-channel laser diodes (LD) controller. The irradiance of the light sources was maintained at 1 mW/cm² across all wavelengths. This power can restore IPPG signal on the mice control skin without causing any damage to the skin. Considering that mice have thinner skin compared to humans, we minimized the optical power to ensure a difference in penetration depth within the mice skin tissue. The camera used was a dual-camera equipped with dual channels, featuring both visible and near-infrared image sensors (FS-1600D-10GE; JAI, Miyazaki, Japan). The visible and near-infrared light entering the camera are separated by a dichroic mirror and directed to their respective sensors as in Fig. 1b. The lens (67716; Edmund Optics, New Jersey, U.S.) was positioned in front of the camera to focus on the target, and the measurement distance was approximately 25 cm. The schematic diagram of the imaging system is shown in Fig. 1c, and the experimental system is set up as shown in Fig. 1d.

Process of acquiring IPPG signals for each wavelength using the system

Figure 2 shows a custom-designed graphical user interface (GUI) (in Fig. 2a) for image acquisition using a dual-camera and the process for acquiring IPPG signals (in Fig. 2b) through multi-wavelength imaging in a burn lesion model. The light source used in the experiment was a four-wavelength laser system, which was switched by an LD controller and irradiated at four different wavelengths. The dual-camera captured images at 35 fps with a resolution of 1440 × 1080 pixels. The field of view (FOV) was 4.8 × 3.65 cm². Images were acquired for 5 s per wavelength using custom-designed GUI. Each wavelength's images were stored in separate channels and image processing was performed individually using MATLAB. Region of interest (ROI) corresponding to the burn area were selected in the images, and the average pixel values within the ROI were stored in each wavelength channel. These average values reflect the amount of light absorbed, which is affected by changes in blood volume over time. Discrete wavelet transform (DWT) was applied to remove baseline drift (DC component) present in the raw IPPG signals, and then the signals were smoothed using a moving average filter. Therefore, we visualized the sinusoidal IPPG signal by plotting the intensity average over time[34]. IPPG signals obtained from the control skin were observed to be detectable at all wavelengths. That is, IPPG signals were obtained at four wavelengths, from the blue wavelength, which penetrates the least under the skin, to the near-infrared wavelength, which penetrates deep into the tissue.

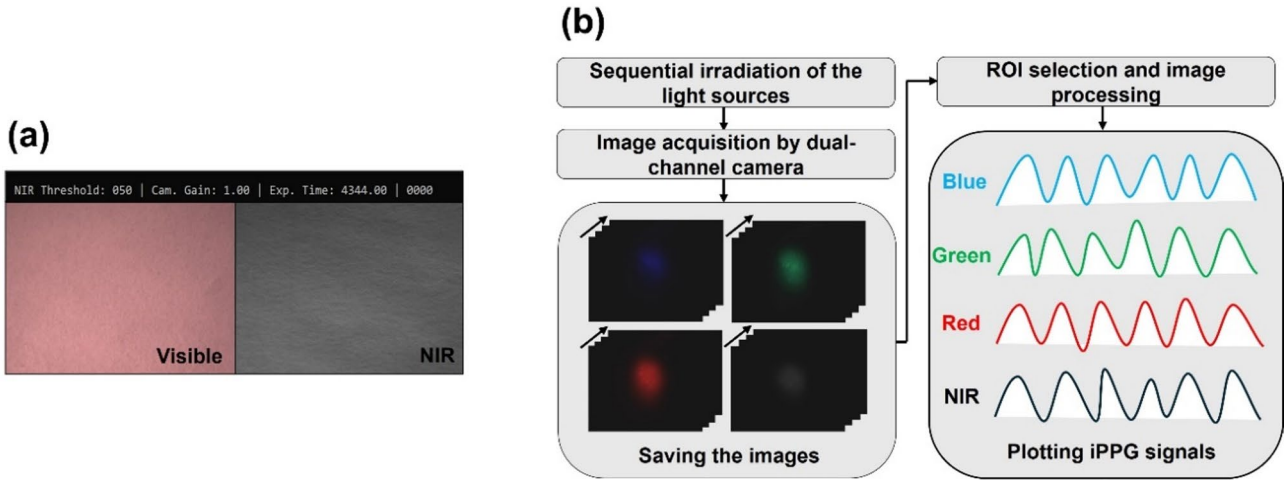

Fig. 2. The process of acquiring IPPG signals at each wavelength (**a**) Custom-designed graphical user interface (GUI) displaying visible and near-infrared images on a split screen, with a field of view (FOV) of 4.8×3.65 cm^2. (**b**) Block diagram including the process of acquiring IPPG signals through multiple wavelengths imaging in burn lesion models.

Creating mouse models by burn severity

To verify the performance of the developed burn severity assessment system, burn models corresponding to the first-, second-, and third-degree were created. In mice, first-degree burns, confined to the epidermis, measure approximately 10–20 μm in depth, second-degree burns extending into the dermis range from 400 to 600 μm, and third-degree burns reaching the subcutaneous tissue are 800 μm or more[35]. Animal experimental models are important tools for assessing the severity of burns, and mice are commonly used in burn research because of their short wound healing time[36,37]. In our experiments, 7-week-old hairless mice (SKH1-hr; Orientbio, Seongnam, Korea) weighing 31–34 g were used to create burn lesion models. Animal experiments were approved by the Dankook University Institutional Animal Care and Use Committee (DKU-24-036) and euthanasia was performed using CO_2 gas in accordance with the animal experiment approval. All experiments were performed in accordance with the relevant guidelines and regulations, including the ARRIVE guidelines and the standard protocol of the Institutional Animal Care and Use Committee (IACUC) of the Ministry of Food and Drug Safety. Before inducing burns, mice were anesthetized with a mixture of Zoletil 50 (30 mg/kg; tiletamine + zolazepam) and Rompun (10 mg/kg; xylazine). Burns were created by placing a cylindrical soldering iron (LedSol-300; EXSO, Busan, Korea) with a diameter of 5 mm vertically on the back of the mouse. The first-degree burn was created by heating the soldering iron at 70 °C for 1 s, second-degree burn was created by heating at 100 °C for 1 s, and third-degree burn was created by heating at 100 °C for 60 s. Before assessing the burn depth, the mice were sacrificed to obtain histological images to confirm whether the burn level was appropriately created at each depth. The histological images were stained with hematoxylin & eosin (H&E) and photographed under a microscope to analyze burn severity. A total of 9 mice were used in the experiment, with 3 mice sacrificed to histologically validate the burn lesion model and establish the conditions for the burn injuries. The remaining 6 mice were used for the IPPG analysis, with 2 repetitions performed on each of the first-, second-, and third-degree burn lesion models. These repeated experiments were conducted to ensure the replicability of the results.

Results

Histological verification for burn severity assessment

To evaluate burn depth using our system, we analyzed histological images after inducing burns in mice to verify that first-, second-, and third-degree burn models were accurately established. Figure 3 shows histological images corresponding to the classification of the generated burn lesions. The first-degree burn is limited to epidermis damage, and the thermal stimulus caused by the burn weakens the skin barrier, resulting in partial peeling of the stratum corneum, as indicated by the red arrow in Fig. 3a[38]. In the normal skin, the dermis shows a typical basket-shaped collagen fiber pattern. However, in the second-degree burn, the dermis is damaged, the basket-shaped pattern is broken, and the collagen fibers are abnormally thickened or randomly arranged (indicated by the green dashed circle in Fig. 3b). In addition, the tissue contraction caused by heat intensifies the eosin staining[39,40]. The depth of tissue damage is approximately 500 μm at most in the histological image of the second-degree burn. In the case of the third-degree burn, the damage extends to the subcutaneous tissue. In normal muscle tissue, the polygonal arrangement of muscle fibers is evenly distributed, whereas after burns, this polygonal structure is lost (indicated by the yellow dashed circle in Fig. 3c)[41]. The depth of tissue damage is approximately 1.25 mm at most in the histological image of the third-degree burn. Through pathological analysis, temperature and time settings corresponding to burn severity in mouse experiments were established. Using these conditions, burn lesion models were created, and the developed system was verified to be able to evaluate the burn depth. In addition, we observed how IPPG signal changed as the burn healed.

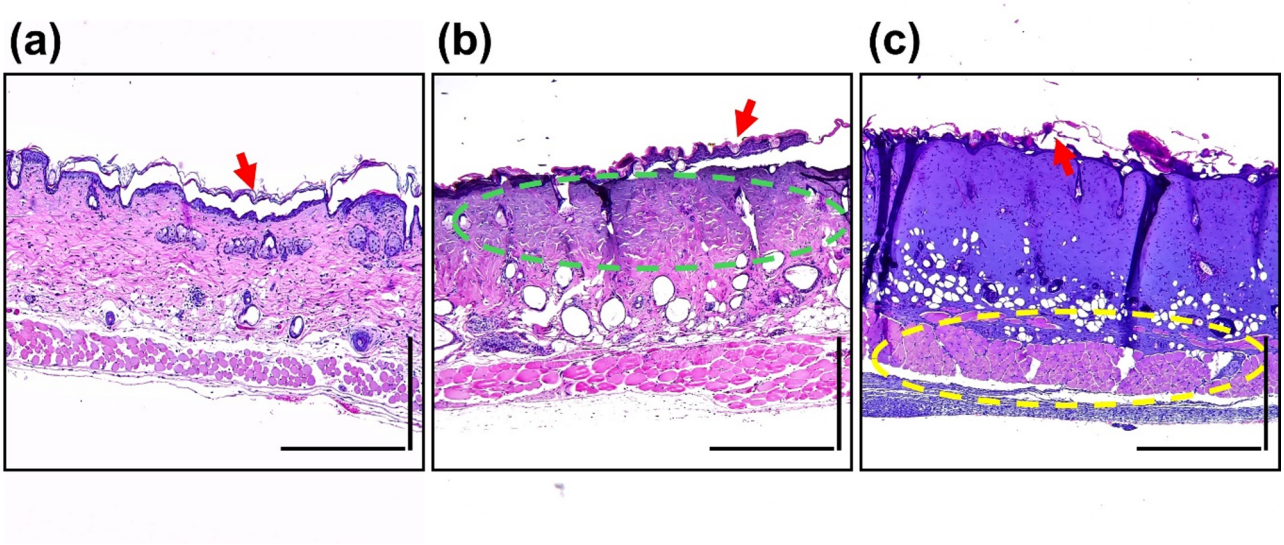

Fig. 3. Histological images according to burn lesion classification (**a**) First-degree burn; the red arrow indicates partial desquamation of the stratum corneum. (**b**) Second-degree burn; the green dashed circle indicates the disruption of the basketweave arrangement of collagen fibers and their abnormal thickening due to dermal damage. (**c**) Third-degree burn; the yellow dashed circle indicates the loss of the polygonal arrangement of muscle fibers. Scale bar = 500 μm.

Burn severity and recovery assessment through wavelength-specific blood flow analysis of the burn area

First, IPPG signals were measured from the control skin before inducing burns, and then the points where burns were to be induced in the mice were designated. Then, three burn degrees (first-, second- and third-degree) created by setting the appropriate temperature and time in the designated area and IPPG signals were measured immediately (0 h) and 24 h later. After 24 h, IPPG signals were measured every 2 days to minimize the risk of death due to excessive anesthesia in the mice. As shown in Fig. 4a, the first-degree burn was visually confirmed in the early stage of the burn and recovered to almost normal appearance on the third day. Figure 4b shows IPPG signals measured at each wavelength in the first-degree burn area for 3 days. In this burn, IPPG signals were consistently obtained without damage at all wavelengths from the induction of the burn to the recovery. These results indicate that the first-degree burn is limited to epidermal damage and does not affect the underlying blood vessels.

Figure 5a shows the progress of wound healing in the mouse model with the second-degree burn for 7 days. In the initial stage, the wound appeared white or yellow due to edema. From the fifth day, the edema began to subside, and a scab formed on the wound surface, accompanied by hyperemia around the wound edge[42–44]. No damage to blood vessels at different depths was observed with the naked eye. Figure 5b shows the results of measuring IPPG signals at various wavelengths in the burn area of the second-degree burn for 7 days. Immediately after the burn injury, IPPG signals at all wavelengths were measured, indicating that blood vessels were not damaged at the time of the burn. However, after 24 h, damaged IPPG signals of blue and green wavelengths were observed, as indicated by the transparent red boxes in Fig. 5b. This suggests that blood vessels were damaged to a depth reached by the green wavelength, with necrosis gradually progressing over time. This pattern is consistent with an earlier report that blood vessel damage does not occur immediately after a burn injury, but that necrosis gradually occurs thereafter[45]. On the fifth day, IPPG signals confirmed the restoration of blood vessels corresponding to the green penetration depth as the wound healed. On the seventh day, IPPG signal at the blue wavelength had also recovered, confirming the restoration of superficial blood vessels.

Figure 6a shows the progress of wound healing in the mouse model with the third-degree burn for 9 days. Immediately after the injury, the center of the wound becomes red due to blood vessels and undergoes progressive ischemia and necrosis. After 24 h, hyperemia was observed at the wound edge. From the fifth day, a scab began to form on the wound surface[46,47]. Figure 6b shows the results of measuring IPPG signals at various wavelengths in the burn area of the third-degree burn for 9 days. Although some blood vessel damage greater than that observed in the second-degree burn was present immediately after the injury, resulting in weaker signals (shown as transparent yellow boxes in Fig. 6b), IPPG signals were still detected at all wavelengths. This is consistent with the results of previous research[48]. However, after 24 h, as the blood vessels gradually became necrotic, IPPG signals at the blue and green wavelengths could no longer be confirmed. On the third day, as necrosis extended to the depth corresponding to the red wavelength, IPPG signals at the red wavelength were also damaged. On the fifth day, the recovery of IPPG signals at the green and red wavelengths indicated the restoration of blood vessels in the deeper layers of the skin as the wound healed. On the ninth day, IPPG signal at the blue wavelength had also recovered, confirming the restoration of superficial blood vessels.

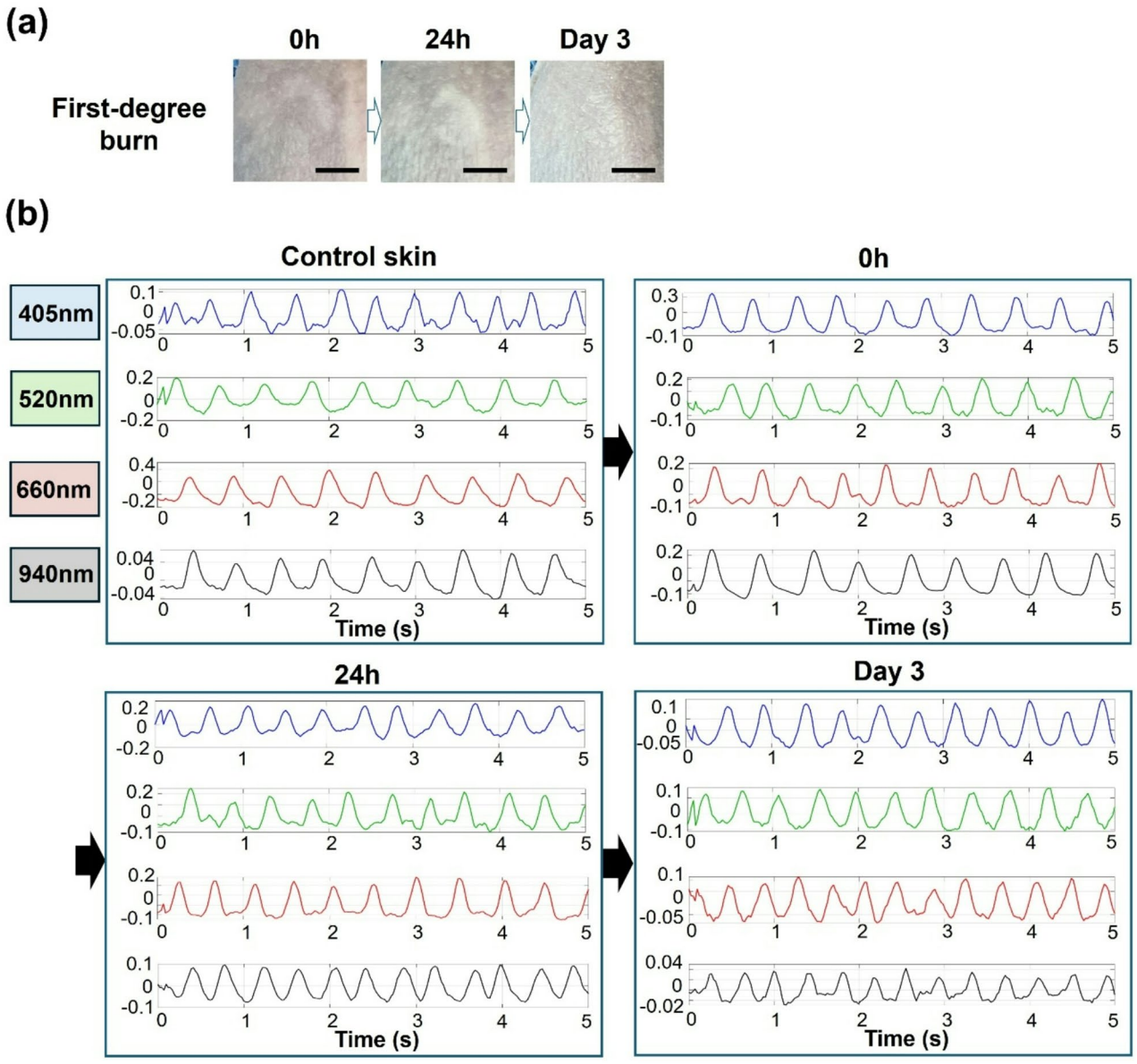

Fig. 4. (**a**) Captured images showing the progression of wound healing in the mouse model with the first-degree burn for 3 days. Scale bar = 0.5 cm. (**b**) IPPG signals at different wavelengths in the burn area of the first-degree burn over 3 days. In the first-degree burn, it was confirmed that IPPG signals were not damaged at any wavelength.

Table 1 shows IPPG signal damage levels at various wavelengths according to the experimental results. In the first-degree burn, the signals were confirmed at all wavelengths from injury to recovery, indicating that the burn was limited to the epidermis and that the blood vessels inside were not damaged. In the second-degree burn, the signals in the blue and green wavelengths were damaged. The tissue damage in the second-degree burn reaches approximately 500 μm, extending to the dermis, indicating blood vessel damage at the depth that the blue and green wavelength can penetrate. In the third-degree burn, the signals were damaged at the blue, green, and even red wavelengths. The tissue damage in the third-degree burn reaches approximately 1.25 mm, extending to the subcutaneous tissue, indicating that the blood vessels were damaged to the depth that the red wavelength, which penetrates deeper, can reach. The results showed consistency across repeated experiments, with identical outcomes observed in each trial (see Supplementary Fig. S1, S2 and S3). Although there were slight variations in the exact timings of signal distortion between two repeated experiments, the overall pattern of signal disruption remained consistent throughout all trials. In this way, the non-contact, non-invasive image-based burn severity measurement system presented in this paper demonstrated to classify burns using IPPG signals from a burn lesion model in mice.

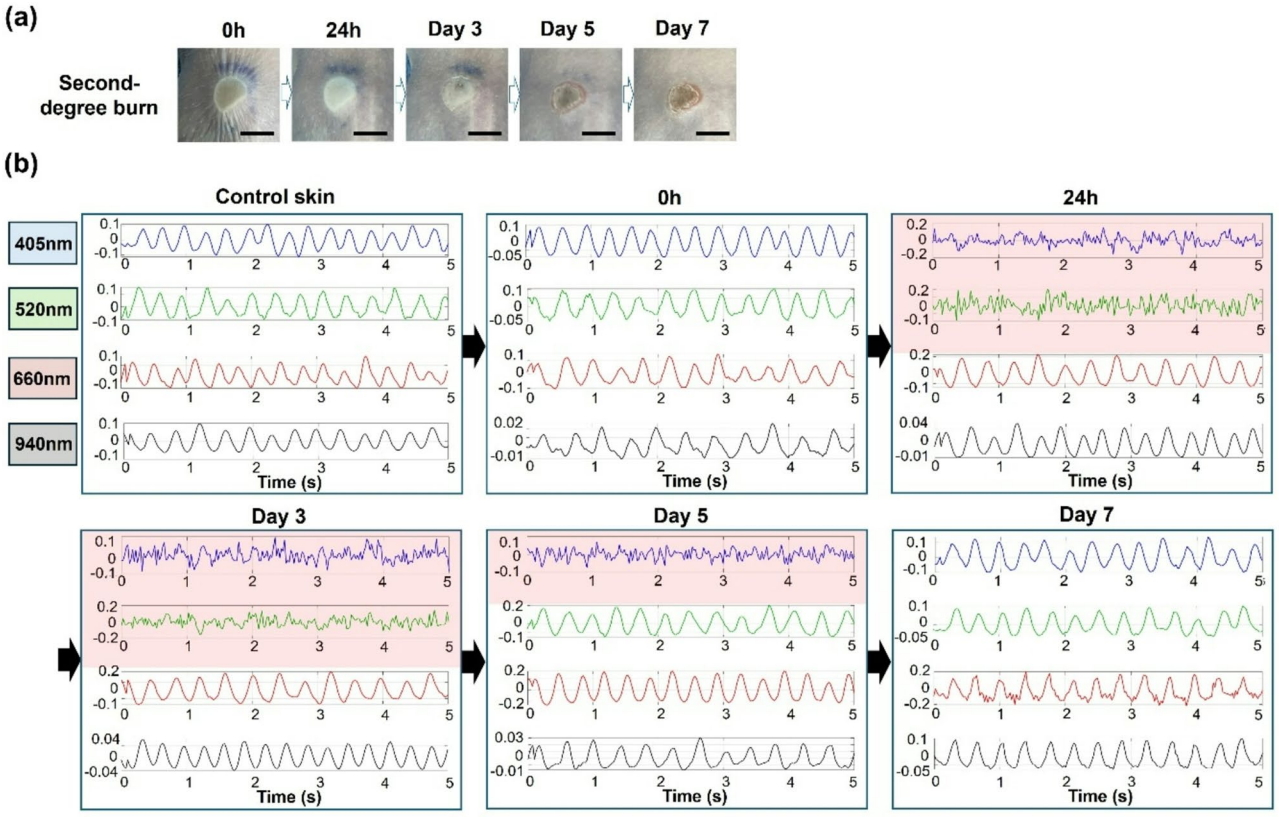

Fig. 5. (**a**) Captured images showing the progression of wound healing in the mouse model with the second-degree burn for 7 days. Scale bar = 0.5 cm. (**b**) IPPG signals at different wavelengths in the burn area of second-degree burn over 7 days. The transparent red boxes indicate the damaged IPPG signals. 24 h after the burn injury, IPPG signals at the blue and green wavelengths were damaged. On the seventh day, IPPG signals were restored at all wavelengths, confirming the restoration of the blood vessels.

Discussion and conclusions

We propose a non-contact, non-invasive technique to evaluate burn severity by measuring IPPG signals from burns using a dual-camera and multi-wavelength light sources. Considering the characteristic that the penetration depth inside the skin varies depending on the wavelength, light sources of various wavelengths were used. The wavelengths used were blue (405 nm), green (520 nm), and red (660 nm) corresponding to visible light and 940 nm corresponding to near-infrared light. The dual-camera has both visible and near-infrared image sensors, so it can detect light of all wavelengths. The system acquires IPPG signals by acquiring images at a speed of 35 fps.

To evaluate the performance of the proposed system, the burn lesion models were created using hairless mice. Burn severity was classified into the first-degree burn limited to the epidermis, the second-degree burn extended to the dermis, and the third-degree burn extended to the subcutaneous tissue. This classification was confirmed through histological analysis to ensure uniformity in the creation of the burn lesion models.

Using the burn lesion models and the proposed system constructed according to the burn severity, IPPG signals were measured from the initial burn to recovery in order to evaluate burn severity. According to the experimental results, normal IPPG signals were observed at all wavelengths in the first-degree burn. This suggests that the burn was limited to the epidermis and did not affect the underlying blood vessels. In the case of the second-degree burn, damaged signals were observed at blue and green wavelengths 24 h after injury. Since this burn affected the dermis, it indicates that blood vessels were damaged to a depth reached by the green wavelength. In the case of the third-degree burn, damaged signals were extended to the maximum red wavelength 3 days after the injury. This burn, which affected the subcutaneous tissue, suggests that blood vessels were damaged to a depth reached by the red wavelength.

A notable observation was that blood flow signals were detected at all wavelengths immediately after the burn occurred. In the case of the second-degree burn, blue and green wavelength signals did not appear 24 h after the burn occurred. This result showed that necrosis of blood vessels corresponding to the penetration depth of green occurred 24 h after the burn. In the case of the third-degree burn, the burn severity was high, and some blood vessels were damaged from the beginning, as evidenced by the fact that the initial IPPG signals were weaker than those observed in other burns. Additionally, 3 days after the burn, signals from not only the blue and green wavelengths but also the red wavelength were not observed, indicating that necrosis of the blood vessels at the depth corresponding to the red wavelength occurred on the third day after the burn. The degree of burn recovery

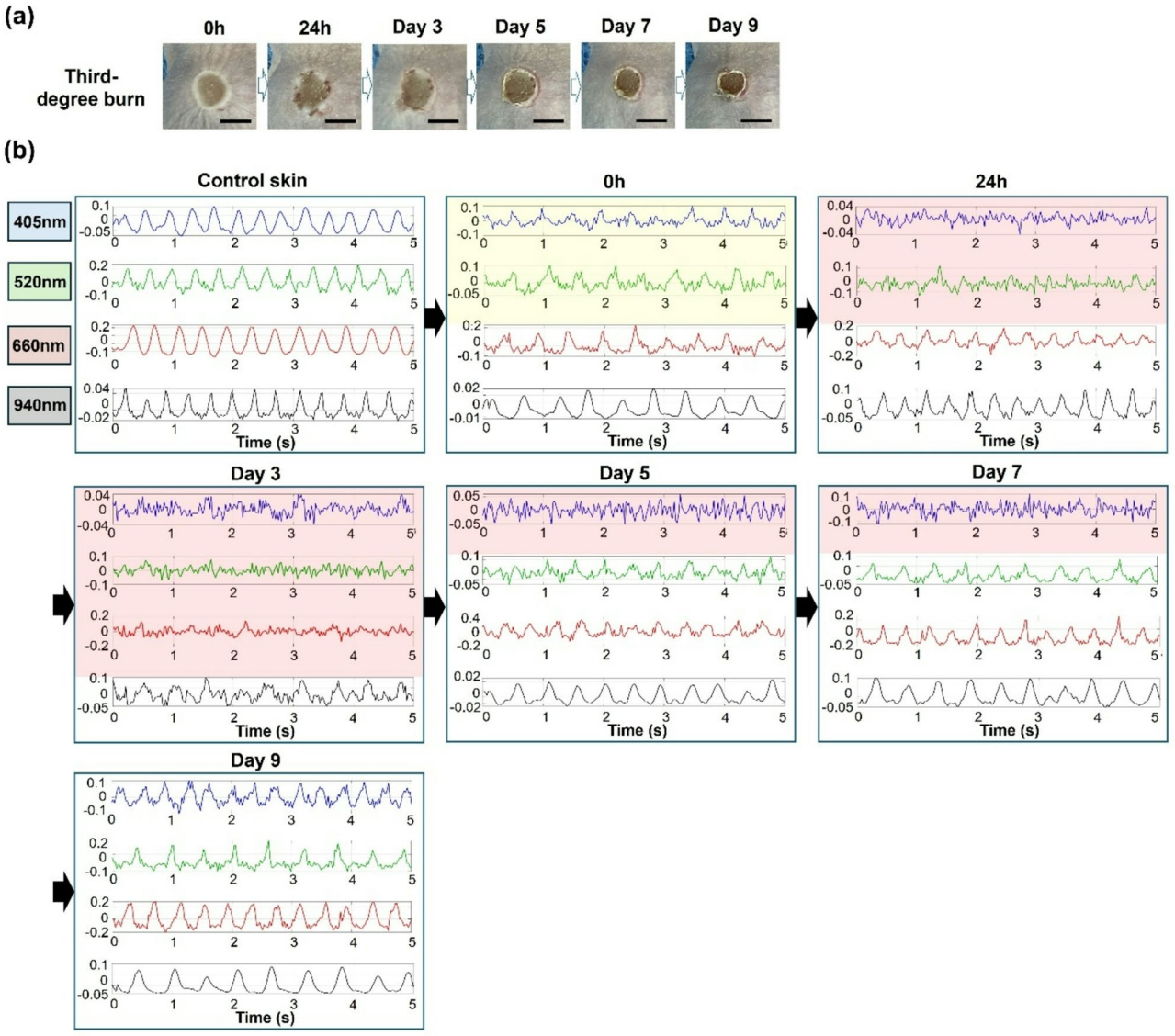

Fig. 6. (**a**) Captured images showing the progression of wound healing in the mouse model with the third-degree burn for 9 days. Scale bar = 0.5 cm. (**b**) IPPG signals at different wavelengths in the burn area of the third-degree burn over 9 days. The transparent yellow boxes indicate weakened IPPG signals and transparent red boxes indicate damaged IPPG signals. The maximum damage to IPPG signals, including those at the blue, green, and red wavelengths, was observed on the third day. On the nineth day, IPPG signals were restored at all wavelengths, confirming the restoration of the blood vessels.

was also confirmed through IPPG signals, with the blue wavelength signal appearing after 7 days for the second-degree burn and after 9 days for the third-degree burn, indicating that blood vessels were completely restored. Angiogenesis is known to deliver nutrients, maintain oxygen homeostasis, and promote cell proliferation and tissue regeneration[49]. Therefore, our system can not only determine burn severity but also help evaluate the extent of burn healing by observing the recovery of damaged IPPG signals based on wavelengths.

The study has certain limitations that need to be addressed. Second-degree burns are the most common burn type, and it is especially important to distinguish between superficial and deep second-degree burns. Misdiagnosis can lead to unnecessary surgery, so it is important to choose a treatment method for optimal healing[50]. However, in our study, it was difficult to accurately distinguish between superficial and deep second-degree burns when creating a burn lesion model due to the individual characteristics of mice. If we differentiated these and created burn lesion models, too many animals would be sacrificed, so we conducted the experiment limited to deep second-degree burns. Furthermore, since our study primarily relies on the qualitative assessment of pulsatile flow, additional quantitative and statistical validation is required to confirm its accuracy and clinical applicability. Future studies should ensure the safety of the system, experimentally verify its effectiveness across various degrees of burns through clinical trials and further assess its applicability to human patients.

Additionally, melanin absorption in the visible spectrum causes the greatest light attenuation effect compared to other chromophores in the skin, such as hemoglobin, water, and lipids. The absorption coefficient for dark

Wavelength	Burn classification		
	First-degree	Second-degree	Third-degree
Blue (405 nm)	No damage	**Damaged**	**Damaged**
Green (520 nm)	No damage	**Damaged**	**Damaged**
Red (660 nm)	No damage	No damage	**Damaged**
NIR (940 nm)	No damage	No damage	No damage

Table 1. Damaging levels of IPPG signals at different wavelengths for each burn classification. Bolded 'Damaged' indicates the wavelengths at which IPPG signal was damaged due to burn injuries. The first-degree burn showed no signal damage across all wavelengths. The second-degree burn showed signal damage at the blue and green wavelengths. The third-degree burn extended signal damage to include blue, green, and even red wavelengths.

skin is 74% higher than for light skin, which can affect light penetration depth[51]. To address this, future research should include individuals with diverse skin tones to better understand wavelength penetration variations and adjust wavelengths accordingly. A real-time skin tone analysis in the camera system could allow for such adjustments or the use of optical filters to selectively transmit specific wavelengths. Moreover, by incorporating methods such as linear regression[52] to address motion artifacts across different wavelength channels, we aim to enhance the accuracy and practicality of the IPPG system, making it applicable in clinical settings where patient movement is inevitable.

Current clinical assessment of burn severity is often subjective and has a significant lack of accuracy. However, the classification of burn severity can have a decisive impact on treatment decisions and prognosis, such as scarring, so accurate assessment of burn severity is essential. The IPPG assessment technique proposed in this study, which utilizes the difference in skin tissue penetration depth according to wavelength, is expected to be an effective tool for assessing burn depth noninvasively and in a non-contact manner, without tissue biopsy.

Data availability

The datasets generated during and/or analyzed during the current study are available from the corresponding author on reasonable request.

Received: 18 February 2025; Accepted: 7 May 2025
Published online: 13 May 2025

References

1. Evers, L. H., Bhavsar, D. & Mailänder, P. The biology of burn injury. *Exp. Dermatol.* **19**, 777–783. https://doi.org/10.1111/j.1600-0625.2010.01105.x (2010).
2. Çakir, B. & Yeğen, B. Ç. Systemic responses to burn injury. *Turk. J. Med. Sci.* **34**, 215–226. https://doi.org/10.1097/00005373-197010000-00008 (2004).
3. Lateef, Z. et al. The cutaneous inflammatory response to thermal burn injury in a murine model. *Int. J. Mol. Sci.* **20**, 538. https://doi.org/10.3390/ijms20030538 (2019).
4. Lu, S. Burn wound healing. *Chin. Burn Surg.* 207–248. https://doi.org/10.1007/978-94-017-85754_9 (2015).
5. Warby, R. & Maani, C. V. *Burns Classification*. *StatPearls* https://www.ncbi.nlm.nih.gov/books/NBK539773/ (2023).
6. Rice, P. & Orgill, D. Assessment and classification of burn injury. 129–132 (2023).
7. Abazari, M., Ghaffari, A., Rashidzadeh, H., Badeleh, S. M. & Maleki, Y. A systematic review on classification, identification, and healing process of burn wound healing. *Int. J. Lower Extrem. Wounds*. **21**, 18–30. https://doi.org/10.1177/1534734620924857 (2022).
8. Monstrey, S., Hoeksema, H., Verbelen, J., Pirayesh, A. & Blondeel, P. Assessment of burn depth and burn wound healing potential. *Burns* **34**, 761–769. https://doi.org/10.1016/j.burns.2008.01.009 (2008).
9. Serrano, C., Boloix-Tortosa, R., Gómez-Cía, T. & Acha, B. Features identification for automatic burn classification. *Burns* **41**, 1883–1890. https://doi.org/10.1016/j.burns.2015.05.011 (2015).
10. Heimbach, D., Engrav, L., Grube, B. & Marvin, J. Burn depth: A review. *World J. Surg.* **16**, 10–15. https://doi.org/10.1007/BF02067108 (1992).
11. Burmeister, D. M. et al. Noninvasive techniques for the determination of burn severity in real time. *J. Burn Care Res.* **38**, e180–e19. https://doi.org/10.1097/BCR.0000000000000338 (2017).
12. Kahn, A. M., Mccrady, V. L. & Rosen, V. J. Burn wound biopsy multiple uses in patient management. *Scand. J. Plast. Reconstr. Surg. Hand Surg.* **13**, 53–56. https://doi.org/10.3109/02844317909013020 (1979).
13. Watts, A. M. I., Tyler, M. P. H., Perry, M. E., Roberts, A. H. N. & McGrouther, D. A. Burn depth and its histological measurement. *Burns* **27**, 154–160. https://doi.org/10.1016/S0305-4179(00)00079-6 (2001).
14. Renkielska, A. et al. Static thermography revisited - An adjunct method for determining the depth of the burn injury. *Burns* **31**, 768–775. https://doi.org/10.1016/j.burns.2005.04.006 (2005).
15. Kamolz, L. P. et al. Indocyanine green video angiographies help to identify burns requiring operation. *Burns* **29**, 785–791. https://doi.org/10.1016/S0305-4179(03)00200-6 (2003).
16. Merz, K. M. et al. Cutaneous microcirculatory assessment of the burn wound is associated with depth of injury and predicts healing time. *Burns* **36**, 477–482. https://doi.org/10.1016/j.burns.2009.06.195 (2010).
17. Kloppenberg, F. W. H., Beerthuizen, G., I. J., M. & Ten Duis, H. J. Perfusion of burn wounds assessed by laser doppler imaging is related to burn depth and healing time. *Burns* **27**, 359–363. https://doi.org/10.1016/S0305-4179(00)00138-8 (2001).
18. Zheng, K. J., Middelkoop, E., Stoop, M., van Zuijlen, P. P. M. & Pijpe, A. Validity of laser speckle contrast imaging for the prediction of burn wound healing potential. *Burns* **48**, 319–327. https://doi.org/10.1016/j.burns.2021.04.028 (2022).
19. Chin, M. S. et al. Hyperspectral imaging for burn depth assessment in an animal model. *Plast. Reconstr. Surg. Glob Open.* **3**, e591. https://doi.org/10.1097/GOX.0000000000000558 (2015).

20. Lai, M. et al. Imaging PPG for in vivo human tissue perfusion assessment during surgery. *J. Imaging.* **8**, 94. https://doi.org/10.3390/jimaging8040094 (2022).
21. Allen, J. Photoplethysmography and its application in clinical physiological measurement. *Physiol. Meas.* **28**, R1. https://doi.org/10.1088/0967-3334/28/3/R01 (2007).
22. Park, J., Seok, H. S., Kim, S. S. & Shin, H. Photoplethysmogram analysis and applications: an integrative review. *Front. Physiol.* **12**, 808451. https://doi.org/10.3389/fphys.2021.808451 (2022).
23. Eaton, A., Vincely, V., Lloyd, P., Hugenberg, K. & Vishwanath, K. The reliability and accuracy of estimating heart-rates from RGB video recorded on a consumer grade camera. *Opt. Biophotonics Low-Resource Settings III.* **10055**, 130–136. https://doi.org/10.1117/12.2252629 (2017).
24. Alhallak, K. & Skin Light and their interactions, an In-Depth review for modern Light-Based skin therapies. *Clin. Dermatol. Ther.* **7**, 1–15. https://doi.org/10.24966/CDT-8771/100081 (2021).
25. Ash, C., Dubec, M., Donne, K. & Bashford, T. Effect of wavelength and beam width on penetration in light-tissue interaction using computational methods. *Lasers Med. Sci.* **32**, 1909–1918. https://doi.org/10.1007/s10103-017-2317-4 (2017).
26. Ray, D., Collins, T., Woolley, S. & Ponnapalli, P. A. Review of wearable Multi-Wavelength photoplethysmography. *IEEE Rev. Biomed. Eng.* **16**, 136–151. https://doi.org/10.1109/RBME.2021.3121476 (2023).
27. Sabino, C. P. et al. The optical properties of mouse skin in the visible and near infrared spectral regions. *J. Photochem. Photobiol. B.* **160**, 72–78. https://doi.org/10.1016/j.jphotobiol.2016.03.047 (2016).
28. Bashkatov, A. N., Genina, E. A., Kochubey, V. I. & Tuchin, V. V. Optical properties of human skin, subcutaneous and mucous tissues in the wavelength range from 400 to 2000 Nm. *J. Phys. D Appl. Phys.* **38**, 2543. https://doi.org/10.1088/0022-3727/38/15/004 (2005).
29. Avci, P. et al. Low-Level laser (Light) therapy (LLLT) in skin: stimulating, healing, restoring. *Semin. Cutan. Med. Surg.* **32**, 41 (2013).
30. Sowers, T., Yoon, H. & Emelianov, S. Investigation of light delivery geometries for photoacoustic applications using Monte Carlo simulations with multiple wavelengths, tissue types, and species characteristics. *J. Biomed. Opt.* **25**, 016005–016005. https://doi.org/10.1117/1.JBO.25.1.016005 (2020).
31. Vincely, V. D. & Bayer, C. L. Photoacoustic imaging of rat kidney tissue oxygenation using second near-infrared wavelengths. *J. Biomed. Opt.* **30**, 026002–026002. https://doi.org/10.1117/1.JBO.30.2.026002 (2025).
32. Hong, G. et al. Through-skull fluorescence imaging of the brain in a new near-infrared window. *Nat. Photonics.* **8**, 723–730. https://doi.org/10.1038/nphoton.2014.166 (2014).
33. Wilson, R. H., Nadeau, K. P., Jaworski, F. B., Tromberg, B. J. & Durkin, A. J. Review of short-wave infrared spectroscopy and imaging methods for biological tissue characterization. *J. Biomed. Opt.* **20**, 030901–030901. https://doi.org/10.1117/1.JBO.20.3.030901 (2015).
34. Park, Y., rim, Shin, Y. & Eom, J. B. Non-contact oxygen saturation monitoring for wound healing process using dual-wavelength simultaneous acquisition imaging system. *Biomed. Eng. Lett.* **13**, 455–463. https://doi.org/10.1007/s13534-023-00275-x (2023).
35. Lin, C. Y. et al. Sex- and age-dependent skin mechanics—A detailed look in mice. *Acta Biomater.* **175**, 106–113. https://doi.org/10.1016/j.actbio.2023.11.032 (2024).
36. Hew, J. J. et al. Mouse models in burns research: characterisation of the hypermetabolic response to burn injury. *Burns* **46**, 663–674. https://doi.org/10.1016/j.burns.2019.09.014 (2020).
37. Cai, E. Z. et al. Creation of consistent burn wounds: A rat model. *Arch. Plast. Surg.* **41**, 317–324. https://doi.org/10.5999/aps.2014.41.4.317 (2014).
38. Yang, Z. *Chinese Burn Surgery* (ed. Zongcheng, Y.) https://doi.org/10.1007/978-94-017-85754 (2015).
39. Kwa, K. A. A. et al. Effective enzymatic debridement of burn wounds depends on the denaturation status of collagen. *Wound Repair. Regener.*. **28**, 666–675. https://doi.org/10.1111/wrr.12827 (2020).
40. Rawlins, J. M., Lam, W. L., Karoo, R. O., Naylor, I. L. & Sharpe, D. T. Quantifying collagen type in mature burn scars: A novel approach using histology and digital image analysis. *J. Burn Care Res.* **27**, 60–65. https://doi.org/10.1097/01.bcr.0000192266.14329.7b (2006).
41. Clark, A. T. et al. Muscle homeostasis is disrupted in burned adults. *J. Burn Care Res.* **41**, 33–40. https://doi.org/10.1093/jbcr/irz190 (2020).
42. Zhang, Y. et al. Role for heat shock protein 90α in the proliferation and migration of HaCaT cells and in the deep second-degree burn wound healing in mice. *PLoS One.* **9**, e103723. https://doi.org/10.1371/journal.pone.0103723 (2014).
43. Okur, M. E. et al. Evaluation of burn wound healing activity of novel fusidic acid loaded microemulsion based gel in male Wistar albino rats. *Saudi Pharm. J.* **28**, 338–348. https://doi.org/10.1016/j.jsps.2020.01.015 (2020).
44. Guo, H. F. et al. Healing properties of epidermal growth factor and tocotrienol-rich fraction in deep partial-thickness experimental burn wounds. *Antioxidants* **9**, 130. https://doi.org/10.3390/antiox9020130 (2020).
45. Clark, R. A. F. et al. Blood vessel occlusion with erythrocyte aggregates causes burn injury progression—microvasculature dilation as a possible therapy. *Exp. Dermatol.* **27**, 625–629. https://doi.org/10.1111/exd.13518 (2018).
46. De Moraes, J. M. et al. Anti-inflammatory effect of low-intensity laser on the healing of third-degree burn wounds in rats. *Lasers Med. Sci.* **28**, 1169–1176. https://doi.org/10.1007/s10103-012-1213-1 (2013).
47. Singer, A. J., McClain, S. A., Taira, B. R., Guerriero, J. L. & Zong, W. Apoptosis and necrosis in the ischemic zone adjacent to third degree burns. *Acad. Emerg. Med.* **15**, 549–554. https://doi.org/10.1111/j.1553-2712.2008.00115.x (2008).
48. ORDER, S. E., MASON, A. D., SWITZER, W. E. & MONCRIEF, J. A. Arterial vascular occlusion and devitalization of burn wounds. *Ann. Surg.* **161**, 502–508 (1965).
49. Rodrigues, M., Kosaric, N., Bonham, C. A. & Gurtner, G. C. Wound healing: A cellular perspective. *Physiol. Rev.* **99**, 665–706. https://doi.org/10.1152/physrev.00067.2017 (2019).
50. Jaskille, A. D., Shupp, J. W., Jordan, M. H. & Jeng, J. C. Critical review of burn depth assessment techniques: part I. historical review. *J. Burn Care Res.* **30**, 937–947. https://doi.org/10.1097/BCR.0b013e3181c07f21 (2009).
51. Setchfield, K., Gorman, A., Simpson, A. H. R. W., Somekh, M. G. & Wright, A. J. Effect of skin color on optical properties and the implications for medical optical technologies: a review. *J. Biomed. Opt.* **29**, 010901–010901. https://doi.org/10.1117/1.JBO.29.1.010901 (2024).
52. Chizari, A., Schaap, M. J., Knop, T., Seyger, M. M. B. & Steenbergen, W. Mitigation of motion artifacts in handheld laser speckle contrast imaging illustrated on psoriasis lesions. *IEEE Trans. Biomed. Eng.* **72**, 70–78. https://doi.org/10.1109/TBME.2024.3438375 (2024).

Acknowledgements

This research was supported by Basic Science Research Program through the National Research Foundation of Korea (NRF) funded by Ministry of Education (grant number : RS-2021-NR066334); by the Korea Medical Device Development Fund grant provided by the Korea government (the Ministry of Science and ICT, the Ministry of Trade, Industry and Energy, the Ministry of Health & Welfare, the Ministry of Food and Drug Safety) (Project No. 1711174973, RS-2022–00166898); and by a grant of the Korea Health Technology R&D Project through the Korea Health Industry Development Institute (KHIDI), funded by the Ministry of Health & Welfare, Republic of Korea (grant number : RS-2023-KH136789).

Author contributions

J.B.E conceived the study and took the lead in project management and supervision. Y.P designed the study, collected, and analyzed the data. J.B.E and Y.P wrote and reviewed the manuscript.

Declarations

Competing interests

The authors declare no competing interests.

Additional information

Supplementary Information The online version contains supplementary material available at https://doi.org/10.1038/s41598-025-01707-7.

Correspondence and requests for materials should be addressed to J.B.E.

Reprints and permissions information is available at www.nature.com/reprints.

Publisher's note Springer Nature remains neutral with regard to jurisdictional claims in published maps and institutional affiliations.